MODIFICATION TO THE IRON ABUNDANCE ALGORITHM BASED ON MOON MINERALOGY MAPPER IMAGER ON-BOARD CHANDRAYAAN-1. M. Bhatt[1], U. Mall[1], C. Wöhler[2], R. Bugiolacchi[1], A. Berezhnoy[3] and A. Grumpe[2]. [1]Max Planck Institute for Solar System Research, 37191, Katlenburg-Lindau, Germany (bhatt@mps.mpg.de). [2]Image Analysis Group, TU Dortmund University, 44227 Dortmund, Germany, [3]Sternberg Astronomical Institute, Moscow State University, Moscow, Russia.

Introduction: Iron is a key element for studies of the origin and geologic evolution of the Moon. Iron in terms of FeO weight present (wt.%) is measurable remotely using the absorption band parameters of visible/near-infrared (VIS-NIR) reflectance spectra. Several algorithms have been proposed to detect FeO wt.% by utilizing the 1-µm absorption band parameters for the Clementine and telescopic datasets [e.g., 1–5]. Most of the empirical models relying on mineralogical measurement techniques are based on minimizing the space weathering effects from the mineralogical composition of the uppermost surface layer. Recently a new algorithm has been proposed in [6] which relies on the 2-µm absorption parameters utilizing the data from the Infra-red Spectrometer, SIR-2 [7] and the Moon Mineralogy Mapper (M^3) [8] on-board Chandrayaan-1 [9]. In [6], the M^3 spectra were normalized to the reflectance at 1.5 µm, but no further photometric or topographic correction was performed, such that discrepancies of up to 4 wt.% FeO in comparison to the SIR-2 FeO map of the same region occurred.

In this study, we have modified the iron abundance estimation equation in [6] for M^3 data by applying photometric and topography corrections. This modified algorithm is applied to the crater Tycho and its surrounding as a test of the modified algorithm. We compare our results with the Clementine based FeO wt.% map generated using the algorithm in [2] and the regression–based approach [10] relying on M^3 data. Furthermore, we introduce a correction of the estimated FeO content for TiO_2

M^3 based FeO abundance estimation algorithm: Based on the method in [11], the M^3 radiance data [12] have been photometrically and topographically corrected using the Hapke model [13] and the GLD100 [14], and a 20 pixels per degree global reflectance mosaic has been prepared. Bonpland D crater in Mare Cognitum (10.1°S 18.2°W, Fig. 1a) region has been selected as a calibration site. The 2-µm band depth (BD2) vs. normalized continuum slope (CS2) relation has been derived according to [6] (Fig. 1b), where the resulting slope coefficient is used for computing an empirical calibration between the band parameters and laboratory FeO wt.% measurements [6]. The accordingly modified FeO content corresponds to

$$\mathrm{FeO\ (wt\%)} = 70.02 \times (\mathrm{BD2} + 0.56 \times \mathrm{CS2}) - 6.725 \quad (1)$$

Based on Eq. (1), we constructed a FeO map of the western lunar nearside region from 40° W to 5° E and 55° S to 55° N. A second FeO map and a TiO2 map were derived using [10], which is an extension of the regression-based approach [5] relying on Lunar Prospector elemental abundances [15] as a reference (cf. [4] for a regression approach relying on different spectral parameters). We used the minimum wavelength, depth, width and continuum slope of the 1-µm band and the depth and continuum slope of the 2-µm band for FeO estimation, and the 1-µm continuum slope and the logarithm of the ratio between the 1-µm and 2-µm absorption depths for TiO2 estimation. The difference between the two constructed FeO maps is linearly correlated with the estimated TiO2 content with a correlation coefficient of 0.82, leading to a TiO2-corrected 2-µm band based FeO abundance according to

$$\mathrm{FeOcorr\ [wt\%]} = \mathrm{FeO} + 1.647 \times \mathrm{TiO2} - 4.300 \quad (2)$$

The correction for TiO2 according to Eq. (2) is used here instead of the sample-based correction introduced in [3] and applied in [6].

Iron abundance map of Tycho and its surroundings: Fig. 2 presents a comparative study of the crater Tycho (43.4°S 11.1°W) and its surroundings. The SIR-2 iron abundance map has been generated using 39 equidistant tracks using equation (4) from [6] (Fig. 2c). Accordingly, the M³ FeO wt.% map is generated using Eq. (1) (Fig. 2d). The FeO maps constructed based on algorithm [6] using SIR-2 and M³ data, respectively, are consistent with each other. The M³-based TiO_2 map is shown in Fig. 2f, the FeO map corrected for TiO_2 in Fig. 2e. The result of the Clementine-based FeO abundance algorithm in [2], which relies on the 750 nm reflectance and the 950/750 nm ratio, is shown in Fig. 2a. The M³-based FeO map constructed using [10] is shown in Fig. 2b. Its appearance is very similar to the Clementine-based FeO map. Our comparative analysis shows that the FeO abundance estimated using [6] qualitatively shows the same trend as the FeO map derived from Clementine data [2] and from M^3 data [10]. The algorithm in [6] is less sensitive to the topography than the approach in [2]. Furthermore, the FeO map in Fig. 2d constructed based on the 2-µm band parameters reveals stronger variations of the FeO abundances than the FeO maps in Fig. 2a and 2b. In the mare regions in

the northern part of the test region (Mare Humorum and Mare Nubium), Eq. (1) estimates 2–6 wt.% less FeO for mare regions than the methods in [2] and [10]. In the FeO map corrected for TiO_2 according to Eq. (2), the systematic deviations between the FeO estimation algorithm based on the 2-µm band parameters alone and the approaches including the 1-µm band parameters are reduced significantly. We conclude that the TiO2 content has an influence on the shape of the 2-µm absorption band which affects the FeO abundance values inferred from its parameters.

Summary: The FeO abundance estimation algorithm [6] based on the 2-µm absorption band has been modified for photometrically and topographically corrected M³ data. After applying the modified algorithm, the M³ FeO abundance shows a better match with the FeO abundance estimated for SIR-2 data. Our comparative analysis of the Tycho region using three different algorithms shows qualitatively similar FeO variations. Taking into account the TiO2 content reduces the systematic deviations between the 2-µm band based FeO estimation algorithm and the approaches including the 1-µm band parameters.

References: [1] Lucey P. G. et al. (1995), Science 268, 1150–1153; [2] Lucey P. G. et al. (2000) *JGR* 105, 20297-20306; [3] Le Mouélic S. et al. (2000) *JGR* 105, 9445–9456; [4] Shkuratov Y. G. et al. (2005) *PSS* 53, 1287–1301; [5] Wöhler C. et al. (2011) *PSS* 59, 92–110; [6] Bhatt M. et al. (2012) *Icarus* 220, 54-60; [7] Mall U. et al. (2009) *Current Science* 96, 506–511; [8] Pieters C. M. et al. (2009) *Current Science* 96, 500–505; [9] Goswami J., Annadurai M. (2009) *Cur-rent Science* 96, 486–491; [10] Grumpe A. et al. (2012) *Proc. 3rd Moscow Solar System Symp.*; [11] Grumpe A., Wöhler C. (2011) *Proc. 7th IEEE Int. Symp. Image and Signal Proc. and Anal.*, 609-614; [12] http://pds-imaging.jpl.nasa.gov/volumes/m3.html; [13] Hapke, B. (2002) *Icarus* 157, 523–534; [14] Scholten, F. et al. (2012) *JGR* 117, E00H17; [15] http://www.mapaplanet.org/explorer/moon.html.

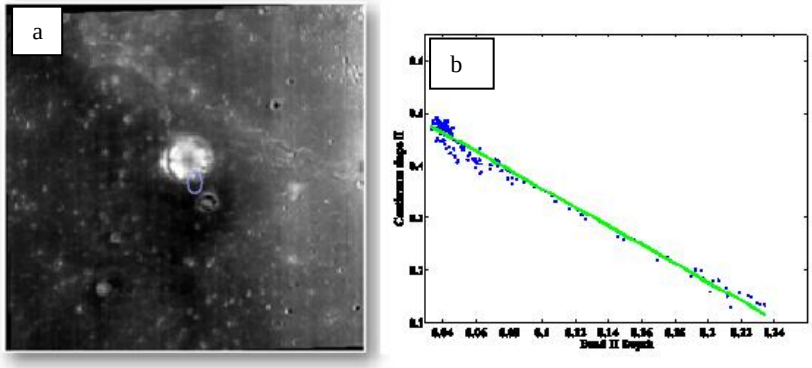

Figure 1: (a) Photometrically and topographically corrected M³ 1579 nm reflectance mosaic of the region around Bonpand D. (b) Correlation plot of the normalized continuum slope versus the 2-µm absorption band depth. The band parameters are extracted from the reflectance spectra from the area marked in (a).

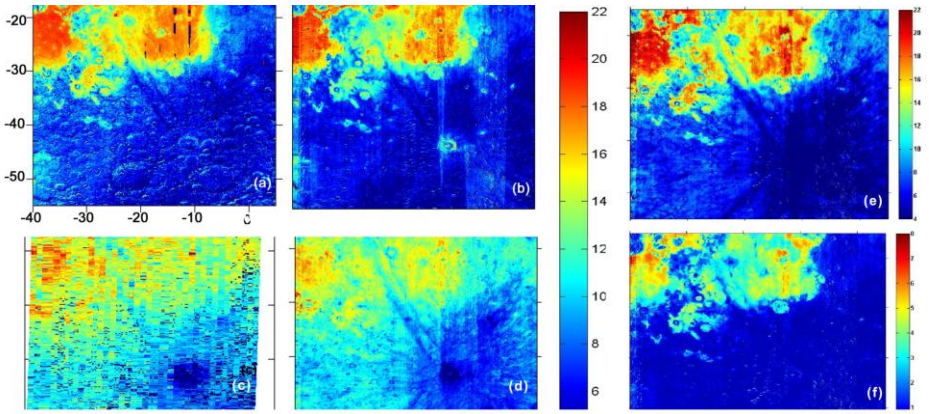

Figure 2: FeO abundance maps of the crater Tycho and its surroundings based on (a) Clementine data using [2]; (b) M³ data using [10]; (c) SIR-2 data using [6]; (d) M³ data using Eq. (1); (e) M³ data using Eqs. (1) and (2). (f) TiO2 map obtained using [10].